SANDIA REPORT
SAND2011-8143
Unlimited Release
Printed October 2011

Nanoparticle Modifications of Photodefined Nanostructures for Energy Applications

Xiaoyin Xiao, D. Bruce Burckel, David R. Wheeler, Cody M. Washburn, Susan M. Brozik, and Ronen Polsky

Prepared by
Sandia National Laboratories
Albuquerque, New Mexico 87185 and Livermore, California 94550

Sandia National Laboratories is a multi-program laboratory managed and operated by Sandia Corporation, a wholly owned subsidiary of Lockheed Martin Corporation, for the U.S. Department of Energy's National Nuclear Security Administration under contract DE-AC04-94AL85000.

Issued by Sandia National Laboratories, operated for the United States Department of Energy by Sandia Corporation.

Available to DOE and DOE contractors from
U.S. Department of Energy
Office of Scientific and Technical Information
P.O. Box 62
Oak Ridge, TN 37831

Telephone: (865)576-8401
Facsimile: (865)576-5728
E-Mail: reports@adonis.osti.gov
Online ordering: http://www.osti.gov/bridge

Available to the public from
U.S. Department of Commerce
National Technical Information Service
5285 Port Royal Rd
Springfield, VA 22161

Telephone: (800)553-6847
Facsimile: (703)605-6900
E-Mail: orders@ntis.fedworld.gov
Online order: http://www.ntis.gov/help/ordermethods.asp?loc=7-4-0#online

SAND2011-8143
Unlimited Release
Printed October 2011

Nanoparticle-Modification of Photodefined Nanostructures for Sensor and Energy Applications

Xiaoyin Xiao, D. Bruce Burckel, David R. Wheeler, Cody M. Washburn, Susan M. Brozik, and Ronen Polsky

Sandia National Laboratories
Albuquerque, NM 87185

ABSTRACT

The advancement of materials technology towards the development of novel 3D nanostructures for energy applications has been a long-standing challenge. The purpose of this project was to explore photolithographically defineable pyrolyzed photoresist carbon films for possible energy applications. The key attributes that we explored were as follows: 1) Photo-interferometric fabrication methods to produce highly porous (meso, micro, and nano) 3-D electrode structures, and 2) conducting polymer and nanoparticle-modification strategies on these structures to provide enhanced catalytic capabilities and increase conductivity. The resulting electrodes were then explored for specific applications towards possible use in battery and energy platforms.

Contents

_Toc209349917

1. PYROLYSIS OF 2D AND 3D INTERFEROMETRICALLY PATTERNED RESIST STRUCTURES

1.1 Introduction

Elemental carbon occurs in two crystalline forms, sp^2 bonded graphitic carbon and sp^3 bonded diamond-like carbon. Despite being composed of the same element, these two distinct allotropes possess widely varying physical properties. Graphite is conductive, opaque and soft, while diamond is insulating, transparent and hard. Pyrolytic carbon formed by pyrolysis of organic polymers is an amorphous form of carbon, existing as a non-crystalline material with local domains of graphitic and diamond like carbon, and hence shares some of the physical properties of both graphite and diamond. Most photo-patternable organic resists (positive and negative tone as well as epoxies such as SU-8) can be converted to carbon through pyrolysis in a reducing atmosphere and has generated a long history of published research [1-4]. One of the distinct advantages of using a resist as the carbon source is that the resist can be patterned prior to conversion to carbon, yielding an elegant approach to structured carbon materials. Much of the research into pyrolyzed resist has focused on the massive increase in conductivity which occurs in going from the insulating resist at room temperature to nearly metallic DC conductivities when pyrolyzed above 1100 °C.

This paper focuses on the conversion of sub-micrometer resist patterns created using interferometric lithography (IL). The ability to pattern materials on the sub-micrometer scale enables many technologically relevant processes, such as optical diffraction, access to interesting mass-transport regimes in solution based chemical reactions, and increased surface area. The ability to combine the attractive physical properties of sub-micrometer patterning with the inherently interesting material properties of pyrolytic carbon enables many varied applications. Here we highlight the use of pyrolyzed IL patterns in two such diverse applications: use of pyrolyzed resist as a growth mask in the metallorganic chemical vapor deposition (MOCVD) growth of gallium nitride (GaN) on sapphire[5], and as an electrochemical electrode in a fuel cell application[6].

1.2 Interferometric Lithography

Interferometric lithography is a versatile maskless patterning approach where coherent plane waves are caused to overlap in space yielding an interference pattern which is then used to

photopattern resist[7]. Figure 1 contains four schematics for using IL to produce various patterns in resist. Interferring two mutually coherent plane waves with an angle 2 θ between the propagation vectors, where θ is measured relative to the surface normal, yields an interference pattern consisting of an array of vertically oriented lines (a.). Rotating the sample in plane by 90 degrees and performing a second exposure produces a 2-D pattern (b.) Depending on the tone of the photoresist, this pattern manifests as either an array of posts (positive resist) or holes (negative tone resist). Although the threshold-ed aerial exposure consists of a 2-D array of rectangular boxes, the high spatial frequency corners are filtered out, yielding round posts/holes. If the propagation directions of the two beams form differing angles, θ_1 and θ_2 with respect to the surface normal, tilted 1-D patterns can be formed (c.) Finally, three dimensional patterns can be formed by performing 3 or more successive tilted exposures with sample rotation in between. Fig 1d. depicts the exposure geometry used to create nominally FCC patterns in the resist – three tilted 1-D exposures with a 120 degree sample rotation between each exposure.

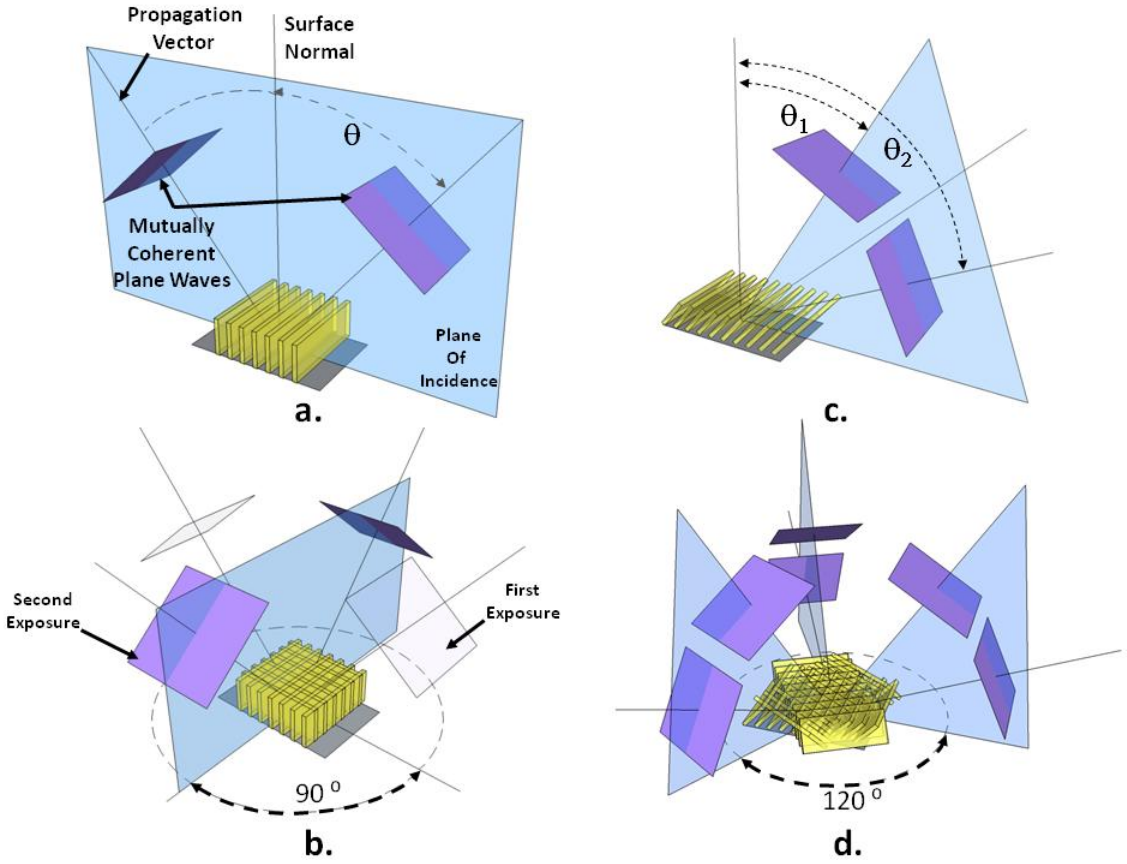

Figure 1. Schematic diagrams indicating the exposure geometry used to create a.) 1-D gratings, b.) a 2-D rectangular array of holes, c.) a tilted 1-D grating, and d.) a 3-D FCC structure.

Figure 2 contains SEM images of several different resist patterns created using these exposure geometries, all formed in SU-8. Figure 2a. shows an array of 1-D lines. The noticeable line width modulation is due to line buckling after cleaving in the marginally cross-linked resist. A more thorough cross linking (increased exposure dose and/or post exposure bake) eliminates this buckling. Fig 2b. contains an SEM image of a rectangular array of 2-D holes with a 2 micron pitch in 20 micron thick resist. The mask-less nature of IL makes creation of high aspect ratio structures (aspect ratio ~ 20) like this possible because the intensity pattern forming the exposure doesn't suffer from diffraction, yielding a constant linewidth over the entire volume over which the interfering beams overlap. It is possible to envision creating the structures in Fig 2a and Fig 2b. using contact lithography, however, attempting to create the structure in Fig 2b using standard lithography with a contact mask would result in significant diffraction at the sub-micron apertures defining the side-walls, resulting in loss of pattern fidelity with increasing depth into the resist. Except for the obvious cleaving related defects, the resist pattern in Fig 2b. maintains a nearly constant linewidth throughout the thickness of the film. Another advantage of using IL to create structures is the ability to make structures with no conventional lithography analog. For instance, it is possible to create structures tilted with respect to the surface normal. The tilted structure in Fig 2c. used two exposures with a 90 sample rotation in order to avoid structural collapse due to drying, but demonstrates the ability of IL to create a structure which cannot be formed via top down conventional lithography. Finally, the 3-D FCC pattern in Fig. 2d. was formed using the three exposure method schematically shown in Fig. 1d. In general, creation of dense arrays of high aspect ratio 1-D lines and 2-D posts are problematic due to capillary forces during drying after development. This problem is alleviated in cross-supported structures like the high aspect ratio 2-D array of holes in Fig. 2b and 2c and the 3-D pattern of Fig. 2d.

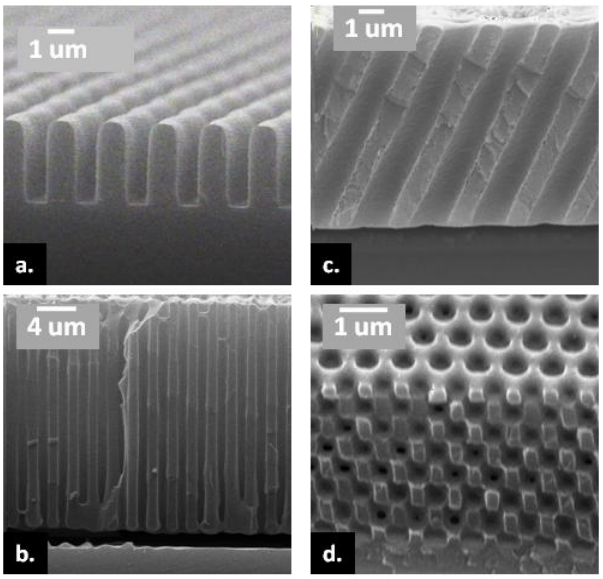

Figure 2. SEM images of resist structures created with IL a.) 1-D gratings, b.) a high aspect ratio 2-D rectangular array of holes, c.) high aspect ratio tilted 2-D array of holes, and d.) a 3-D FCC structure.

1.3 Pyrolysis

Figure 3 contains SEM images of several different pyrolyzed patterns created by pyrolysis of IL-created resist structures like those in Fig 2. We have successfully pyrolyzed structures created in negative tone (NR-7, Futurrex Inc.) positive tone (AZ 4620) and epoxy (SU-8, MicroChem Corp). The patterns were pyrolyzed in a standard tube furnace under flowing forming gas (N_2:H_2, 95:5) and heated to 1050 °C at a ramp rate of 5 °C /min and held isothermal for 1 hour before cooling to room temperature at a similar ramp rate. The reducing atmosphere causes pyrolysis of the photoresist, where non-carbon species in the polymer become volatile and are driven off, leaving predominately carbon. The patterns shrink considerably (60-80%) but, remarkably, maintain their fundamental in-plane morphology and adhesion to the substrate. Figure 3a. shows an array of 1-D lines (NR-7) while Fig 3b. and Fig. 3c show examples of low and high aspect ratio 2-D patterns respectively (SU-8). Fig. 3d contains a top-down SEM image of a 3-D pattern (NR-7).

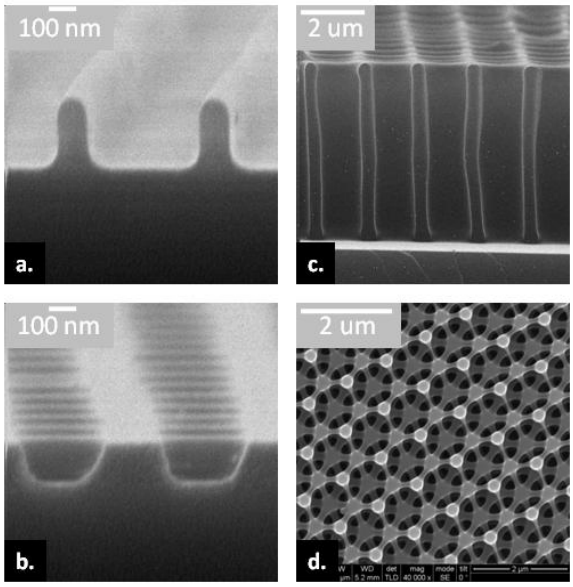

Figure 3. SEM images of pyrolyzed resist structures created with IL a.) 1-D gratings, b.) a low aspect ratio 2-D rectangular array of holes, c.) high aspect ratio 2-D rectangular array of holes, and d.) a 3-D FCC structure.

1.4 Applications

1.4.1 MOCVD of GaN

An application which combines the high temperature stability of the pyrolyzed carbon with the micron scale structuring provided by IL is the use 2-D pyrolyzed patterns as defect reduction growth mask for MOCVD growth of GaN. Group-III nitrides (GaN and AlN) are wide bandgap semiconductors used for making, among other things, blue and UV LEDs and lasers. However growth of these materials is complicated by the fact that bulk GaN and AlN substrates cannot be created in a conventional boule crystal growth approach. Lacking a suitable substrate, GaN epitaxial growth must occur on lattice mismatched substrates which causes a large density of defects and threading dislocations when the film is grown beyond the critical thickness. Research has shown that epitaxial growth on patterned substrates reduces the defect density in the films, however the growth conditions for GaN (~1050 °C under flowing ammonia) make identification of suitable growth mask materials problematic. In addition, the extra patterning steps required to pattern the mask material introduce further opportunities for yield compromise. We explored the use of pyrolyzed patterns as a single step growth mask for MOCVD growth of GaN. Figure 4a. contains an SEM image of the

proof-of-concept growth mask on a sapphire substrate. After a nucleation layer growth step at 530 °C, growth conditions were changed to 1050°C. The cross-section SEM image in 4b. shows a high magnification image of a pyramidal GaN crystal, while the top-down SEM image in Figure 4 c. shows a larger field of GaN crystals. The alignment of the resulting crystal planes on the GaN crystals indicates that the GaN crystal is registered to the sapphire (Al_2O_3) crystal of the substrate. This work demonstrates that the carbon growth mask is capable of surviving the harsh conditions of the GaN MOCVD growth as well as showing moderately good selectivity (relatively few small nucleation sites appear on the carbon template in Fig. 4c.

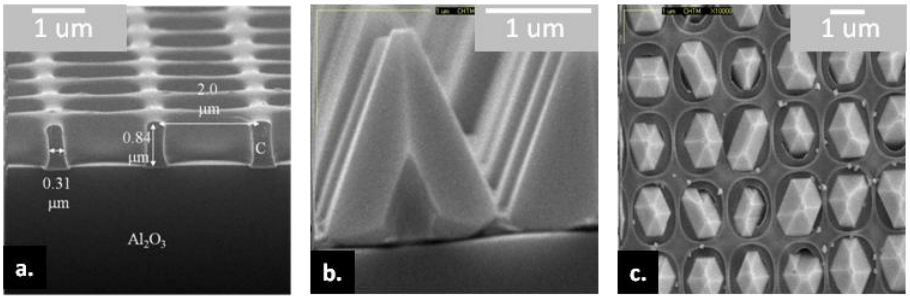

Figure 4.a.) SEM image of pyrolyzed carbon growth mask on sapphire substrate b.) cross section SEM image of a pyramidal single crystal GaN structure grown through pyrolyzed carbon mask, c.) top-down SEM image of GaN crystals growing through carbon growth mask prior to coalescence showing aligned crystal planes (registration to substrate) and good selectivity.

1.4.2 Electrochemical Electrode

Fabrication of engineered 3-D porous carbon electrodes for electrochemical systems such as fuel cells is an application which combines the electrical and surface chemistry properties of the carbon with submicron structuring is the use of IL generated patterns. The SEM image in Fig. 5a shows a high magnification top-down image of a 3-D porous carbon structure. Some of the relevant geometrical dimensions are included in the figure. In Fig. 5b Ag nanoparticles were deposited on the surface of the carbon electrodes using a $AgNO_3/CH_3CN$ system. Using an organic solvent overcomes the hydrophobicity of the carbon structure, allowing wetting throughout the entire volume of the structure in contrast to our previous work using aqueous based Au nanoparticle deposition. Finally, Fig. 5c shows a top down SEM image of an Ag-decorated carbon matrix which was placed in a $PdCl_2$+ascorbic acid/($10CH_3CN+1H_2O$)

solution to electrolessly deposit Pd on the Ag NPs decorating the surface. These Pd-Ag decorated 3-D carbon electrodes demonstrate catalytic activity toward methanol oxidation.

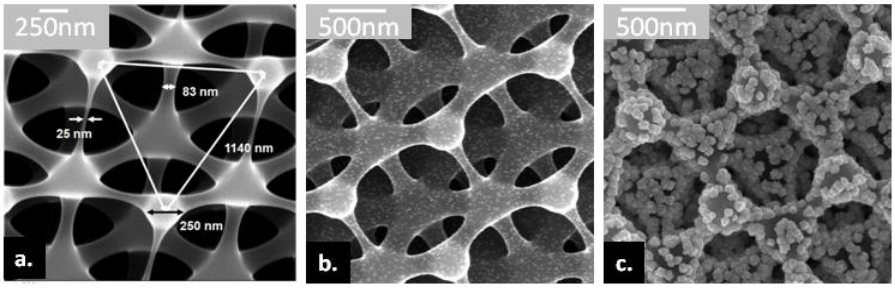

Figure 5 a.) 3-D porous carbon electrode b.) 3-D carbon matrix decorated with electro-deposited Ag nanoparticles, c.) 3-D carbon matrix with Ag NPs coated with Pd in an electroless deposition process.

1.5 Conclusion

We have shown that pyrolysis of IL generated resist structures is an elegant method for the creation of carbon structures with sub-micrometer scale geometry. The approach leverages the unique patterning capability of IL with the inherently useful properties of carbon. The resulting pyrolytic carbon has excellent thermal stability, is structurally resilient in solution based experiments, and electrochemically behaves as glassy carbon, the standard electrode material of choice due to its wide potential window. To demonstrate this functionality, we highlighted two applications which leverage different physical properties of the converted structures.

1.6 References

1. A. M. Lyons, J. of Non-Cryst Solids, **70**, 99, (1985).

2. O. J. A. Schueller, S. T. Brittain and G. M. Whitesides, Adv Mater, **9**, 477, (1997).

3. A. Singh, J. Jayaram, M. Madou, S. Akbar, J. Electrochem. Soc. **149** E78 (2002).

4. C.L. Wang, L. Taherabadi, G.Y. Jia , M. Madou , Y.T. Yeh , B. Dunn , Electrochem. Solid-State Lett. **7** A435 (2004).

5. D. B. Burckel, H.Y. Fan, G. Thaler, D.D. Koleske, J. of Cryst Growth, **310**, 3113, (2008).

6. D. B. Burckel, C. M. Washburn, A. K. Raub, S. R. J. Brueck, D. R. Wheeler, S. M. Brozik, R. Polsky, Small, **5**, 2792, (2009).

7. S. R. J. Brueck, Proc. IEEE, **93**, 1704, (2005).

8. Y. Liu, S. Liu, X. Zhang, *Photonic Crystal Materials and Nanostructures*, (Ed.: R. M. De La Rue), Proc of SPIE 5450, SPIE, Bellingham WA, pp. 473 (2004).

2. INCREASED MASS TRANSPORT AT LITHOGRAPHICALLY DEFINED 3-D POROUS CARBON ELECTRODES

2.1 Introduction

There are many reasons to fabricate nano tailored microstructures. For instance, the nano- and/or microstructuring of electrodes can lead to high surface area, catalytically active interfaces. This structuring has been achieved in many ways: tuning catalytic particle size and shape,[1,2] fabricating catalytic surfaces in porous networks,[3,4,5,6,7] or dispersing catalytic particles into porous templates.[8,9] However, due to small pore diameters, pore nonuniformity, and possible hydrophobicity, diffusion or penetration of electrolyte is rarely uniform in many synthetic (nano)mesoporous materials thereby limiting any advantage increasing the surface area or modifying the structures with functional materials such as catalytic particles or large biomolecules. Another reason to fabricate nano- and/or micro- features is to influence the diffusion-driven mass transport of reactants such as fuels or analytes. Structures containing at least one dimension smaller than the Nernst diffusion layer thickness can experience hemispherical diffusion profiles that result in increased mass transport.[10] While decreasing pore sizes and employing ensembles of smaller structures can provide increased active surface areas, they are often fabricated with a high density that produce overlapping diffusion layers resulting in decreased mass transport (linear diffusion) profiles.[11,12] Thus an inherent trade-off exists between maximizing surface area and preserving favorable hemispherical diffusion characteristics.[13] We report here the fabrication and characterization of 3D carbon electrodes with interconnected porosity that combines the advantages of nanostructuring with increased mass transport. The unique highly ordered nanostructures provide increased pathways for reaction species to diffuse and react throughout entire catalyst-modified electrode surfaces and exhibit microelectrode response characteristics, which we demonstrate to be effective for increased catalytic oxidation of methanol and uncharacteristically uniform deposition of conducting polymer.

We previously published detailed fabrication techniques for 3D carbon substrates, fabricated by means of interferometric lithography.[14] Briefly, commercial photoresist was spin coated on plasma cleaned silicon wafers and exposed to an interference pattern generated by

interfering beams from a Q-switched Nd:YAG laser. This process was repeated iteratively prior to development to generate a multilayer structure. The photoresist was then pyrolyzed at 1100 °C for 1 hour in forming gas (5% H_2 and 95% N_2). The resulting conducting carbon electrode consists of five interconnected layers of ~ 800 nm hexagonal pores. The connecting arms are ~ 80 nm diameter at the top layer and ~300 nm on the bottom layer; the separation distance between individual layers (arms) is approximately 60 nm (detailed images of the top and cross section of the electrodes are shown in supplementary information, Figure s1). Other methods exist for creating porous carbon structures with similar size scales as the patterns presented here, such as templating carbonaceous resins or recorcinol formaldehyde solutions into colloidal silica or polystyrene crystals [14,15]. While the hexagonal porous 3-D carbon electrodes presented here are similar to templated structures, preparing the substrates lithographically does have some advantages. First, the interferometric lithography approach naturally creates large area, defect free patterns, where template approaches suffer from lack of long range order. More importantly, the pore-to-arm ratio of the lithographically prepared substrates can be controlled through exposure dose and development conditions at a fixed lattice spacing which affords the ability to tune the relative size of the pore-to-arm dimension. Finally, the carbon pores presented here are somewhat larger than those that have been reported from colloidal template approaches and provide an excellent platform to study the diffusional mass-transport profiles inside the structures as discussed in the following sections. Pyrolyzed photoresist films are also known to have potential surface chemistry benefits such as atomically flat surfaces with a high degree of hydrogen termination which we have previously demonstrated leads to smaller and more uniform depositions of gold nanoparticles in both planar[16] and IL-fabricated porous films.[17]

2.2 Materials and Methods

Materials and Instruments. All solutions were prepared with 18 MΩ water using a Barnstead Nanopure water purifier (Boston, MA). Isopropanol, Acetonitrile, Methanol, $PdCl_2$, Tetrabutylammoniumtetrafluoroborate (TBATFB), HCl, Pyrrole, $HClO_4$, and H_2SO_4 were purchased from Sigma. Bithiophene was purchased from Kodak. All electrochemical measurements were performed on a CH Instruments 660 Electrochemical Analyzer (Austin, TX) and were measured versus an Ag/AgCl in 3M NaCl reference and a Pt counter electrode

from Bioanalytical Systems (West Lafayette, IN). Scanning electron microscope (SEM) imaging was performed on a Zeiss Supra 55VP field emission gun scanning electron microscope or an FEI Magellan 400 SEM.

Interferometric Lithography of 3D Porous Carbon Electrodes. A bottom anti-reflection coating (BARC), iCON-7 (Brewer Science, Rolla Missouri) was spun onto Silicon wafers at 3000 RPM and baked on a vacuum hotplate at 205°C for 60s. Negative tone NR7 from Futurrex Inc. was used in all of the experiments. A thin layer of NR 7 100P (~ 100 nm) was deposited and spun at 3000 RPM to create an adhesion layer. After flood exposure and post exposure bake at 130 °C on a vacuum hotplate, a thick layer (6μm) of NR7-6000P was deposited and spun at 3000 RPM and soft-baked at 130 °C. The frequency tripled 355 nm line of a Q-switched Nd:YAG laser was used to form the interference pattern. The beam was expanded and split into 2 separate beams and interfered with an angle of 32 degrees between the planewave propagation vectors. The plane of incidence contains both propagation vectors as well as the angle bisector of the propagation vectors, which is tilted with respect to the sample surface normal by 45 degrees. After each exposure the sample is rotated in the plane by 120 degrees and the process is repeated a total of 3 times. After exposure the sample received a post-exposure bake of 85 °C for 2 minutes on the vacuum hotplate. A 120 second puddle development, using RD-6 (Futurrex, Inc) and spin drying completed fabrication of the resist structures. The samples were baked on a hotplate at 180 °C for 30 minutes. The samples were then pyrolyzed at 1100 °C for 1 hour in forming gas (5% H_2 and 95% N_2). Substrates were rinsed with isopropoanol and water before use.

2.3 Results and discussion

Information about diffusional mass transport in the 3D porous carbon structures was examined from the voltammetric response in 1mM ferrocene which is presented in Figure 1. A plot of anodic peak current versus the square root of the scan rate (log i_p versus log $\upsilon^{1/2}$) shows a flat plateau region from 5 to 20 mV/sec followed by a linear region up to 800 mV/sec. At the flat plateau the current is independent of scan rate and is indicative of hemispherical diffusion.[18] This is also shown by the s-shaped voltammogram run at 5 mV/sec (Figure 1 inset, red curve), which is a characteristic of increased mass transport. Other causes of increased mass transport which produce s-shaped voltammograms, such as stirring the solution or using a rotating disk electrode, are not applicable in these experiments and

therefore the voltammogram shape is attributed to hemispherical diffusion similar to what is observed at microelectrodes. The linear portion of the curve from 50 mV/sec to 800 mV/sec is representative of linear diffusion and typically produces peak-shaped voltammograms as shown by the scan at 50 mV/sec (Figure 1 inset, blue curve). Remarkably, the electrode has a profile similar to a microelectrode despite the measured planar area in solution being ~ 0.5 cm^2. The gradual transition from hemispherical to lateral diffusion (or s-shaped to peak shaped voltammograms) upon the increase of scan rate is also typically observed in microelectrodes due to limiting conditions that are dependent on the time scale of the experiment.[19,20] Apparently the pore sizes in our 3D nanostructures are sufficiently large enough to prevent an overlapping of the diffusion layers and preserve hemispherical diffusion at the nanometer scale arms and spokes. To our knowledge, similar diffusion based studies have not been reported using structures prepared from templated polystyrene/silica sphere-based approaches. Hemispherical diffusion profiles are useful in acquiring high mass transport delivery of analytes which we demonstrate with enhanced catalytic methanol oxidation at the 3D porous carbon electrodes after palladium nanoparticle modification.

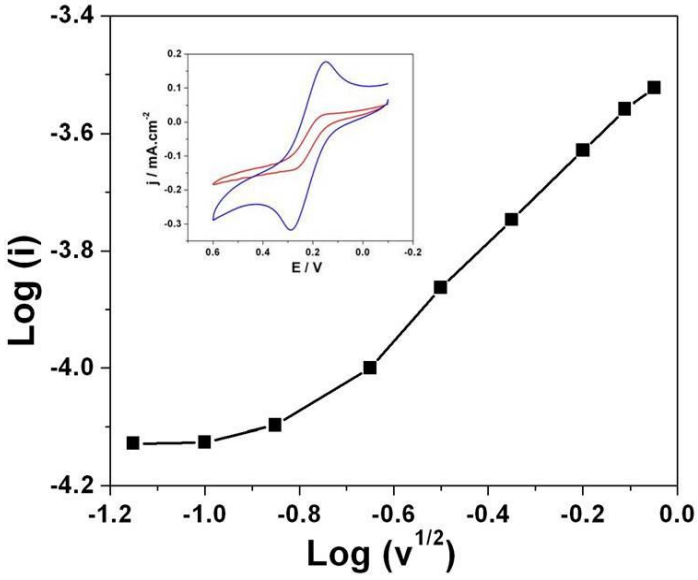

Figure 1. Plot of log current (i) versus log square root of scan rate ($\upsilon^{1/2}$). Inset: Cyclic voltammograms of 3D porous carbon in 1 mM Ferrocene + 0.1 M TBATFB. Scan rate: 5 and 50 mV/s (red and blue line respectively).

Catalytic Pd particles were deposited onto porous 3D carbon electrodes from both aqueous and organic solvent solutions. Deposition at -0.45 V for 100 sec was carried out in a 2 mM Pd/0.5 M H_2SO_4 aqueous solution (versus Ag/AgCl reference and Pt counter electrodes) which resulted in Pd deposition only on the top layers of the structures, as shown in Figure 2A-B. It is presumed that this inhomogeneous deposition is due to the hydrophobic carbon surface which prevents the solution from penetrating into the inner pores, consistent with our previous observation where gold nanoparticles were deposited onto similar structures.[17] Figure 2B shows that Pd particles are densely packed on the top 2 layers with decreased particle deposition on the third layer and no particles deposited on the connecting arms to the fourth layer. On the top 2 layers, most of the Pd particles are 2D clusters, an indication of 2D lateral growth. This is an indication of strong interaction of Pd nuclei with the carbon surface that likely prevents particle-like 3D growth. The particles on the third layer were sparse and unaggregated. The particle sizes and densities were largest on the top layer, and decreased from the second to third layer with the size of individual single Pd particles ranging from about 3 to 10 nm in diameter.

In order to achieve a more complete and uniform surface coverage of Pd particles throughout the entire porous carbon structure, a mixed solvent of acetonitrile (MeCN) and water was explored. MeCN was used to increase surface wettability, while the small amount of water was necessary to dissolve $PdCl_2$. A uniform deposition of Pd nanoparticles throughout the entire porous carbon structures was achieved in a MeCN:water mixture (90:10 vol%) (versus $Ag/AgNO_3$ reference and Pt counter electrodes), as shown in Figure 2C-D. The particle density and morphology is comparable to that shown in figure 2B, indicating that the surface properties of the pyrolyzed carbon, and not the solution composition, dominate in Pd nucleation and subsequent 2D growth.

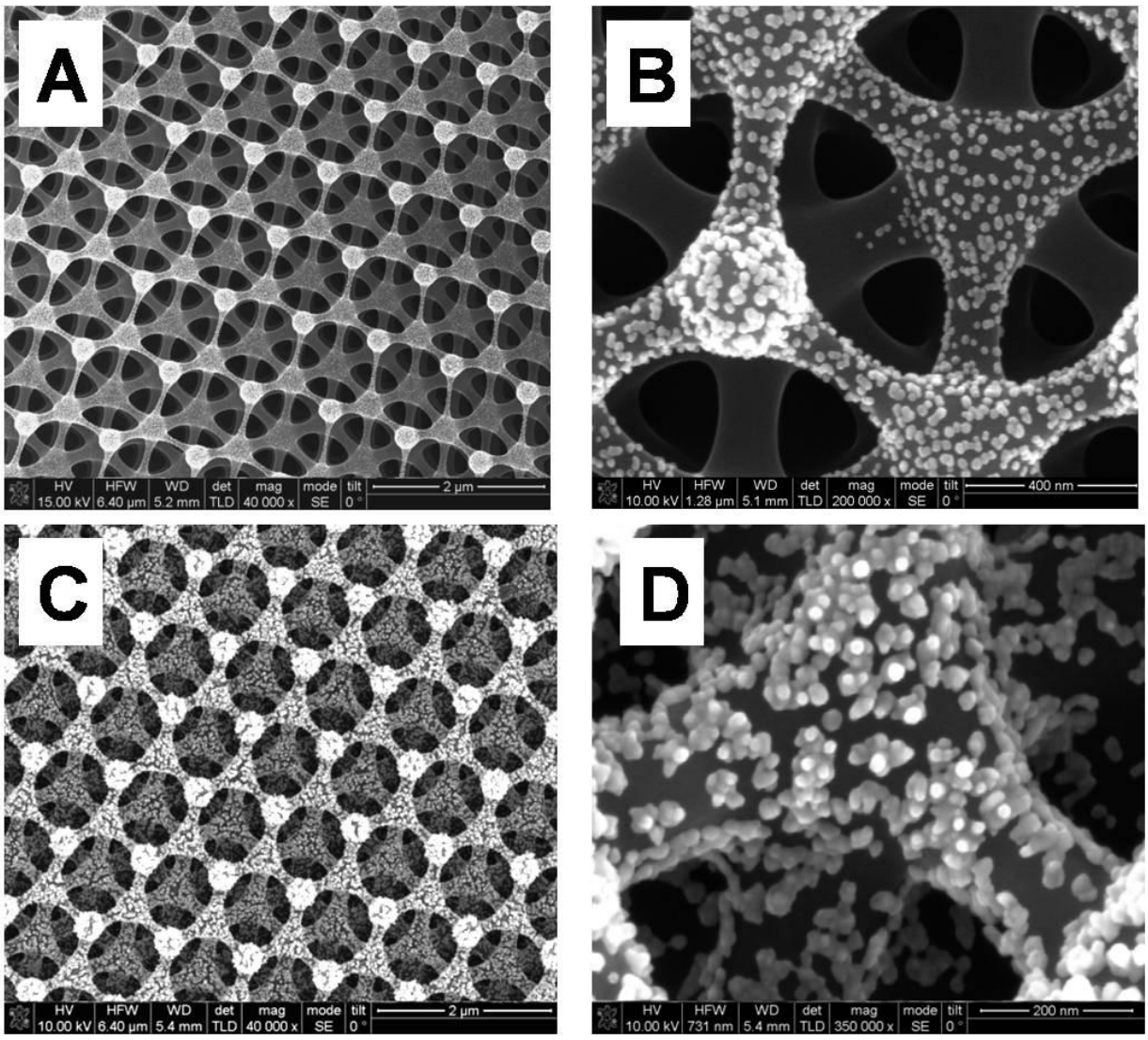

Figure 2. SEM images of Pd deposition onto 3-D porous carbon electrodes at a potential of -0.45 V for 100 sec. (A-B) deposition from 2mM Pd/0.5 M H2SO4, (C-D) deposition from 2 mM Pd/(MeCN + H_2O + 0.1 M HCl). Deposition potential: -0.45 V, deposition time: 100 s.

.

We designate the above two as prepared Pd-modified electrodes shown in Figure 2 A and C as Pd/2D and Pd/3D respectively for ease of description in subsequent discussion. Figure 3 shows the response from cycling in $HClO_4$ and catalytic oxidation of methanol on Pd/3D, Pd/2D, and a glassy carbon electrode (Pd/GC), which was modified with Pd nanoparticles in an identical manner for a control substrate, (blue, red, and black curves respectively). The chemical structure and behavior of pyrolyzed photoresist films resembles that of glassy carbon, consisting of mostly amorphous carbon with small graphitic sp^2 and diamond-like sp^3 regions[21,22] and has similar electrochemical properties.[23] The Pd/2D electrode shows the same amplitude of current as the Pd/GC electrode in both systems indicating that in this case there is not much advantage to the inhomogeneously-coated porous carbon structure as it behaves much like a planar electrode which can be attributed to limited solution accessibility. The Pd/3D electrode, however, shows significant enhancement in catalytic current and in the charge that was transferred from methanol oxidation while exhibiting a positive peak shift which can be attributed to depressed diffusion kinetics. The accessible Pd catalytic surface area at the Pd/3D electrode is about 20 times that of the other two electrodes, as evaluated from the surface oxide desorption wave at ~ 0.4 V (cf. Figure 3A), 0.7×10^{-5} and 1.74×10^{-4} $C.cm^{-2}$, respectively, while the amount of methanol being oxidized increases by a factor of 200, (cf. Figure 3B), 2.2×10^{-5} and 4.6×10^{-3} $C.cm^{-2}$, respectively. If linear diffusion dominated then the current due to methanol oxidation should be proportional to the increase of the surface area. Therefore, since the methanol oxidation at Pd/3D is ten times greater than the increase in surface area over the 2D electrodes the enhancement must be attributed to increased mass transport due to hemispherical diffusion within the nanostructured surfaces.

Another advantage of hemispherical diffusion is demonstrated using the 3D porous carbon structures as a scaffold for the electrochemical deposition of conducting polymers. It is well known that mass transport plays a crucial role in the morphology of electrochemically deposited conducting polymer films whose growth resembles that of metals. Small islands or clusters initially nucleate on the electrode surface and then grow according to a 2-D or 3-D mechanism. The initial grains (or nuclei) eventually overlap and the contiguous film growth proceeds in a 2-D manner for reaction-limited deposition conditions and 3-D for diffusion limited.[24] Conducting polymers often exhibit 2-D growth on microelectrodes due to

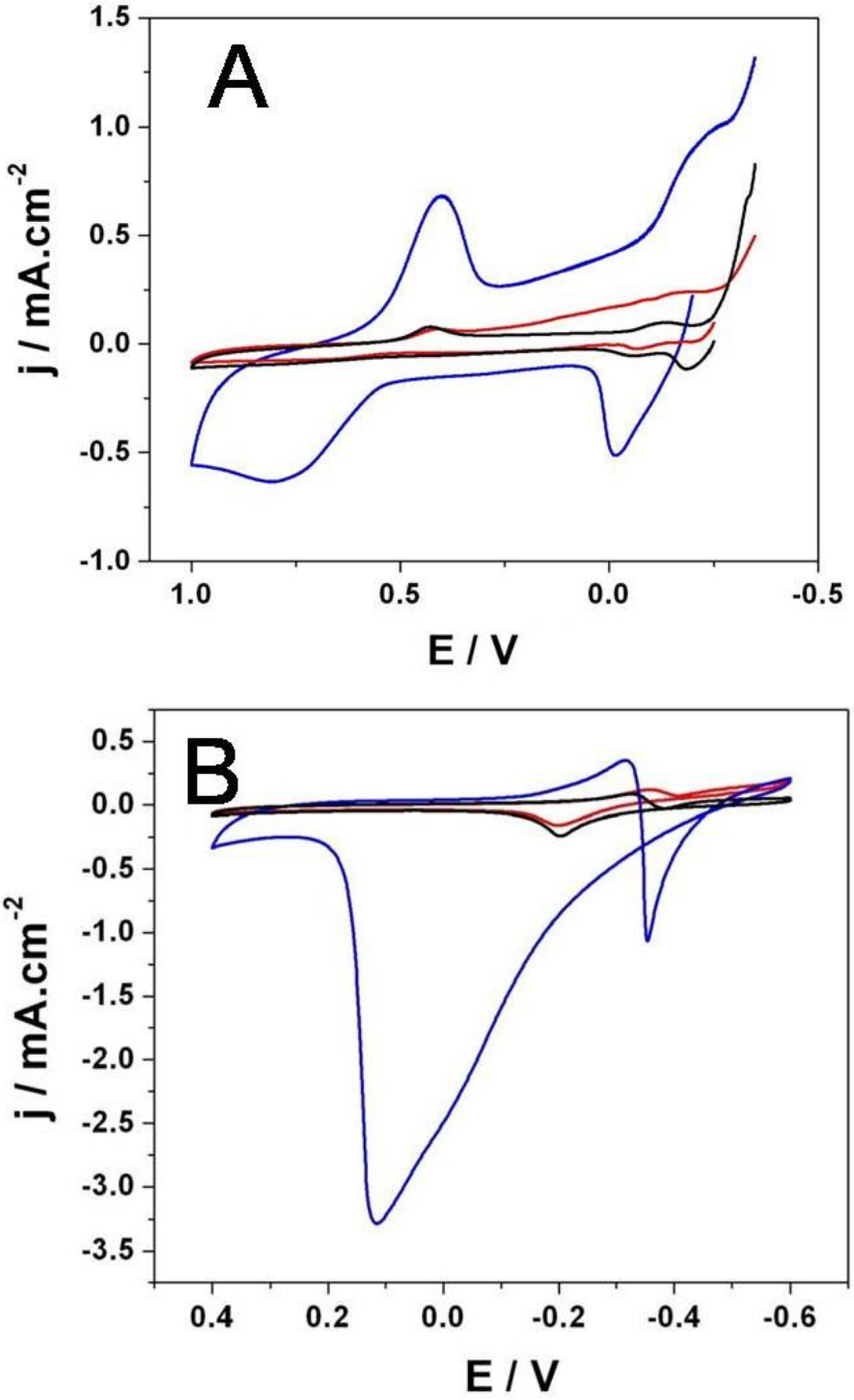

Figure 3. Cyclic voltammograms of Pd/3D (blue), Pd/2D (red), and Pd/GC (black) in 0.5 M $HClO_4$ (A) and 0.5 M NaOH + 0.3 M CH_3OH (B) at a scan rate of 50 mV/s.

hemispherical diffusion of polymer precursors[25] and 3D growth as large asymmetric aggregates diffusion of polymer precursors[25] and 3D growth as large asymmetric aggregates onto bulk electrodes. Fixed potential depositions of 10 mM thiophene in 0.1M $LiClO_4$/acetonitrile performed at 0.85 V (versus $Ag/AgNO_3$ reference and Pt counter electrodes) onto the 3-D porous carbon electrodes show unusually smooth and homogeneous films after 30 and 60 sec of deposition when compared to the same depositions onto identical but planar pyrolyzed photoresist films, as shown in Figure 4 A, B, and C respectively. The polymer film thickness can be controlled with increasing deposition time. For instance the SEM images indicate the connecting arms on the top layer increase from ~74 nm diameter to ~ 186 nm after 30 and 60 sec of deposition (Figure 4 A and B respectively). We believe that the steady state mass transport of monomer molecules during deposition leads to the observed uniform 2-D film growth. Poly(pyrrole) also exhibits smooth films when deposited onto the porous carbon similar to poly(bithiophene) shown in Figure 4D. It is worth noting that other groups have observed large asymmetric particle-like structures following poly(pyrrole) deposition onto microstructured pyrolyzed photoresist films[26] indicating that the unique structure of the 3D porous carbon electrodes is responsible for the homogeneous deposition, rather than the material properties of the films. High resolution SEM imaging confirms that the film deposits uniformly throughout the 3-D electrodes while retaining the open porous film structure resulting in an overlaying nanoporous surface morphology on bare pyrolyzed carbon, presented in Figure 5A and B respectively. Therefore, two regions of hierarchical porosity can be created to maximize surface area, via nanostructuring onto the extended porous network, and still take advantage of hemispherical diffusion through the open pores. The film growth and thickness can also be precisely controlled by cyclic voltammametric deposition. As shown in Figure 6, the increasing current after each successive cycle indicates electrochemical film growth of bithiophene films, while the SEM images of the films electrochemically grown after 0, 2, and 5 potential cycles (from 0 to +1 V) show that the film thickness can be increased in a fashion that provides a means to control pore size. The film thickness remains relatively homogeneous at thinner films, however occasional asymmetric 3D polymer growth increases with increasing film thickness. As the film thickness increases, eventually a point is reached where overlapping diffusion layers are

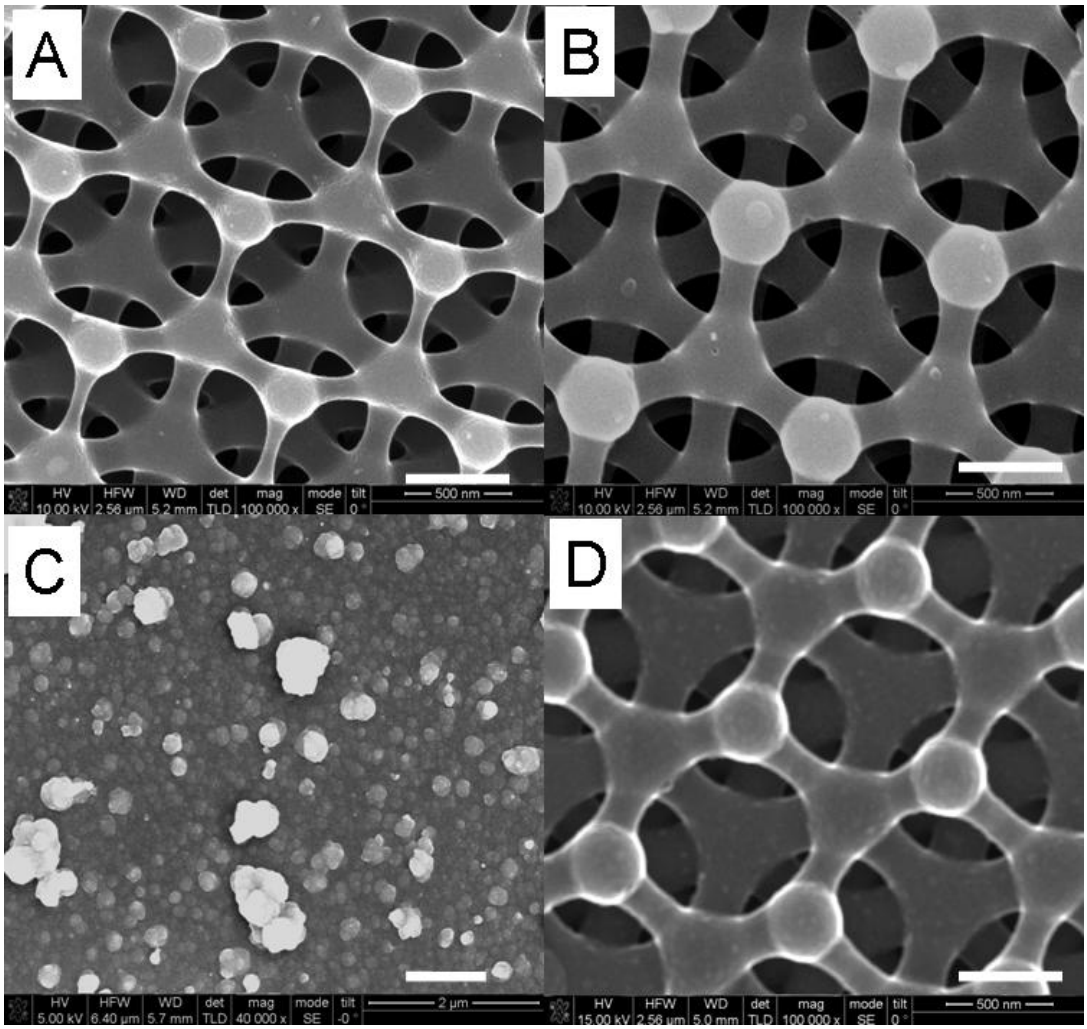

Figure 4**.** (A and B) Scanning electron micrographs of poly(bithiophene) deposition at 850 mV for 30 sec (A) and 60 sec (B). (C) Bithiophene deposition onto planar PPF at 850 mV for 60 sec. (D) Poly(pyrrole) deposited using 2 cyclic voltammograms. Scale bars for (A), (B), and (D) = 500 nm and (C) = 1 µm

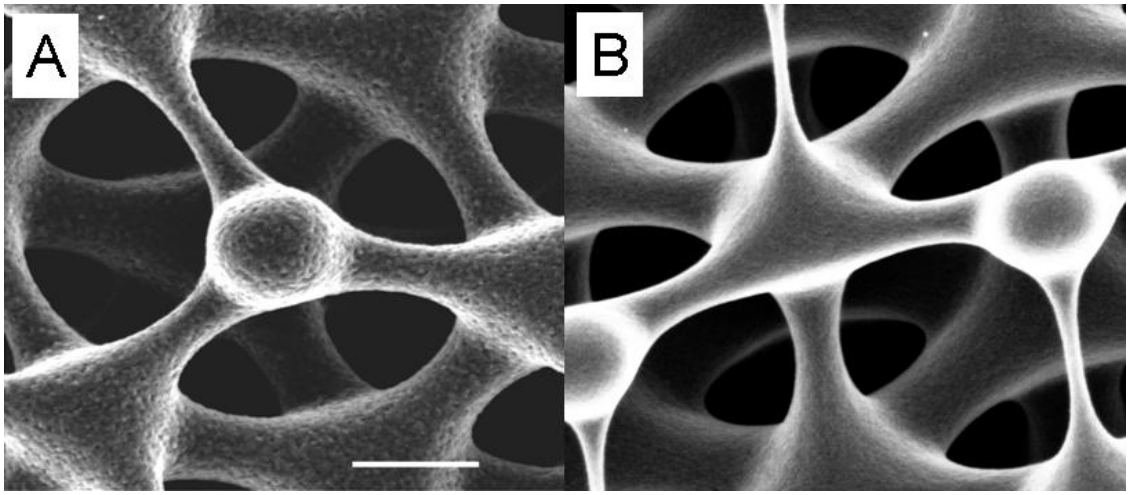

Figure 5. High magnification scanning electron micrograph after 30 sec of bithiophene deposition on porous carbon at 850 mV (A) and bare porous carbon (B). Scale bar = 250 nm

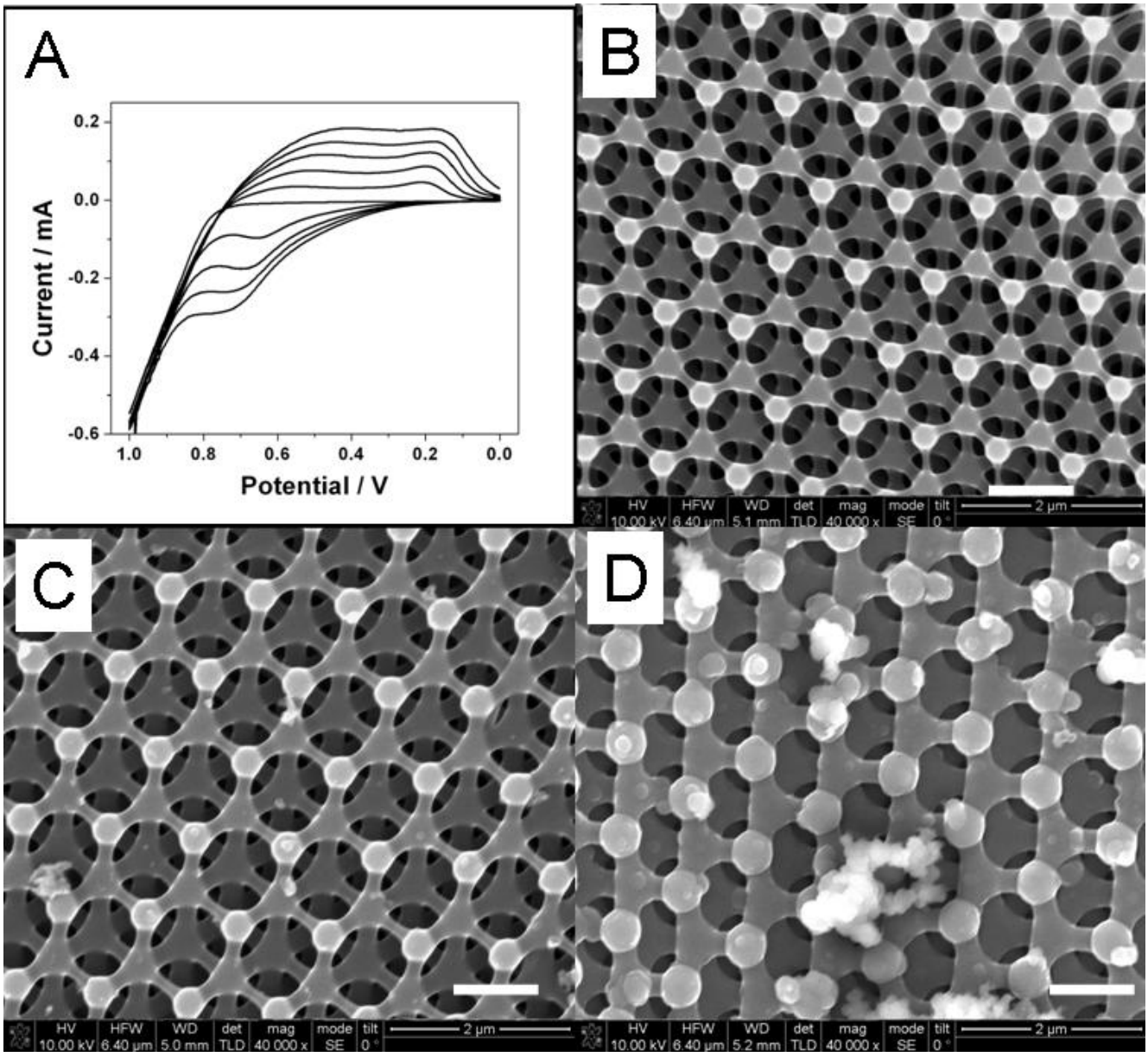

Figure 6**.** (A) Cyclic voltammograms of poly(bithiophene) deposition at a scan rate = 10 mV/sec Scanning electron micrographs of poly(bithiophene) deposition after 0, 2, and 5 cycles (B-D).

created and 3D growth becomes favored, which further supports the purported mechanism that 2D growth is a result of hemispherical diffusion at the porous carbon electrodes.

Cyclic voltammograms obtained in 0.1M $LiClO_4$/acetonitrile at different scan rates after 30 and 60 sec of polymerization at 0.85V are shown in Figure 7 A and B respectively. The electrode fabricated with the 30 sec deposition shows sharp and reversible peaks that increase with increasing scan rates. The 60 sec deposition, in contrast, shows broader peaks and a poorly defined wave as the scan rate approaches 100 mV/sec, indicating a diffusion-limited process within the thicker film. After normalizing the currents to scan rate the electrode prepared from a 30 sec deposition shows little dependence of the peak potential on the scan rate indicating a very efficient doping-undoping process (Figure 7C). The electrode deposited for 60 sec, however, shows a clear dependence of peak potential on scan rate as the process becomes counter-ion diffusion controlled (Figure 7D). At higher scan rates, the charge-compensating ions associated with the oxidation-reduction processes do not have sufficient time to transport through the entire film.

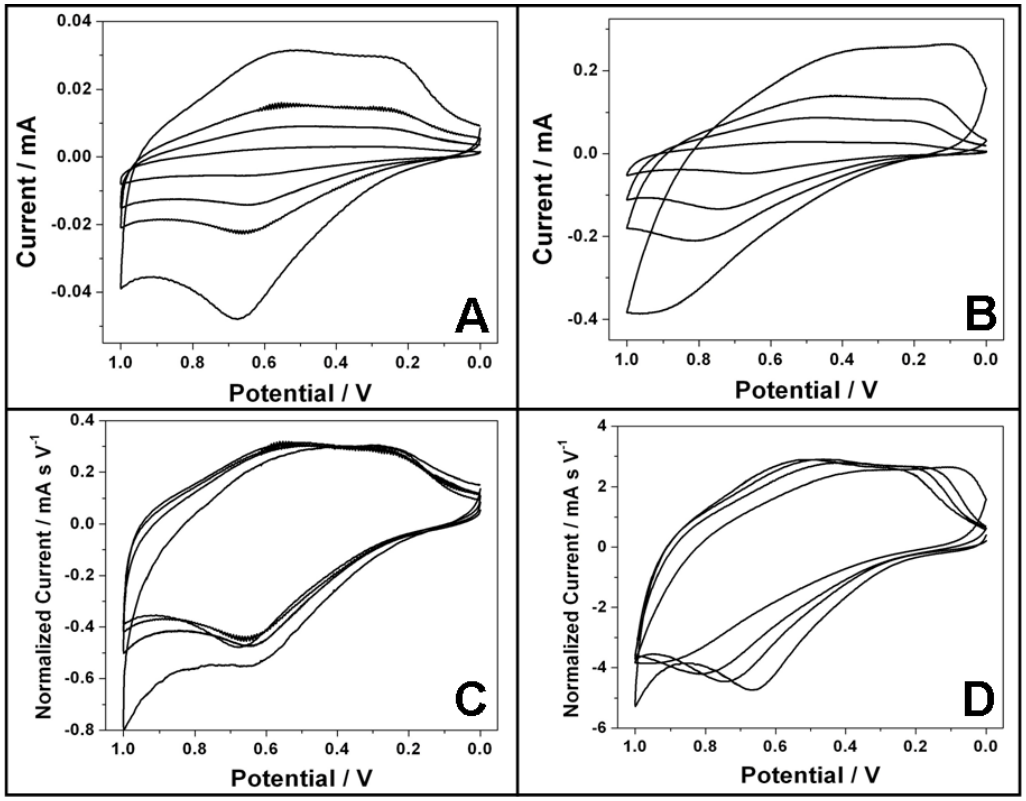

Figure 7 (A and B). Cyclic voltammograms of poly(bithiophene)-modified porous carbon at 10, 30, 50, and 100 mV/sec after 30 and 60 sec deposition respectively at 850 mV. (C and D) Currents normalized to scan rate for 30 and 60 sec deposition respectively.

2.4 Conclusions

In conclusion, we have shown here that the geometry of 3D carbon substrates, defined by interferometric lithography can behave as microelectrodes, exhibiting hemispherical diffusion profiles that can lead to increased mass transport capabilities while maintaining high surface area. Since such 3D porous carbon can be patterned at variable geometries (i.e., number of layers, separation distances between layers, arm diameter, layer thickness, etc.), these electrodes could have many advantages over synthetic (nano)mesoporous materials: 1) optimized pore sizes can be used to promote mass transport into inner pores, 2) they provide 3D high surface area-to-loading capabilities for catalytic nanoparticles leading to the full usage of the catalytic Pd particles over the entire porous structure, and 3) improved morphological film depositions for conducting polymers . We are investigating the opportunities these electrodes could offer in such areas as batteries, supercapacitors, biological sensors and hydrogen storage devices.

2.5 References

1. Tian, N., Zhou, Z., Y. Sun, S., G.;Ding, Y., and Wang Z. L. *Science* **2007**, 316, 732
2. Goodman, D. W. *Nature* **2008**, 454, 948
3. Adams, B., Wu, G., Nigrio, S., and Chen A. *J. Am. Chem. Soc.* **2009**, 131, 6930
4. Kiani, A., and Fard, E. N. *Electrochim. Acta* **2009**, 54, 7254
5. Hakamada, M., and Mabuchi, M. *J. Alloys and Compounds* **2009**, 479, 326
6. Krishnamoorthy, K., and Zoski, C. G. *Anal. Chem*. **2005**, 77, 5068
7. Park, S., Song, Y. J., and Han, J. H. *Electrochim. Acta* **2010**, 55, 2029
8. Niesz, K., Koebel, M., and Somorjai, G. A. *Inorgan. Chim. Acta* **2006**, 359, 2683
9. Chu, S. Z., Kawamura, H., and Mori, M. *J. Electro. Soc.* **2008**, 155, D414

10. Wang, J. *Analytical Electrochemistry*. **2006**, 3rd Ed. Wiley-VCH,

11. Menon, V., and Martin, C.R. *Anal. Chem.* **1995**, 67, 1920

12. De Leo, M., Kuhn, A., and Ugo, P. *Electroanalysis* **2007**, 19, 227

13. Walcarius, A. *Anal. Bioanal. Chem*. 2010, 396, 261

14. Chai, G.S., Yoon, S.B., Yu, J.S., Choi, J.H., and Sung, Y.E., **2004**, 108, 7074

15. Bauman, T.F., and Satcher, J.H. *J. of Non-Crystalline Solids* **2004**, 350, 120

16. Polsky, R., Washburn, C.M., Montano, G., Liu, H.Q., Edwards, T.L., Lopez, D.M., Harper, J.C., Brozik, S.M., and Wheeler, D.R. *Smal*l, **2009**, 5, 2510

17. Burckel, D. B., Washburn, C. M., Raub, A. K., Brueck, S. R. J., Wheeler, D. R., Brozik, S. M., and Polsky, R. *Small* **2009**, 5, 2792

18. (a) Zoski, C., *Handbook of Electrochemistry* **2006**, Elsevier, (b) Davies, T.J., Jones, S.W., Banks, C.E., Campo, J.D, Mas, R., Munoz, F.X., and Compton, R.G., *J. of Electroanal. Chem.* **2005**, 585, 51.

19. (a) Penner, R.M., and Martin, C.R., *Anal. Chem.* **1987**, 59, 2625. (b) Amatore, C., Pebay, C., Thouin, L., Wang, A., and Warkocz, J.S., *Anal. Chem.* **2010**, 82, 6933.

20. (a) Ca, D.P., Sun, L., and Cox, J.A., *Electrochim. Acta* **2006,** 51, 2188, (b) Amatore, C., Pebay, C., Thouin, L., and Wang, A., *Electrochem. Comm.,* **2009**, 11, 1269.

21. McCreery, R.L. *Chem. Rev.* **2008**, 108, 2646

22. Ranganathan, S., and McCreery, R.L. *Anal. Chem.* **2001,** 73, 893

23. Gui, A.L., Liu, G.Z., Chockalingam, M., Saux, Le., Harper, J.B., and Gooding, J.J., *Electroanalysis*, **2010**, 22, 1283

24. J.A. Harrison, and H.R. Thirsk *Electroanal. Chem*..; A.J. Bard, ED.; Marcel Dekker: New York, **1971, 5,** 67.

25. Hwang, B.J., Santhanam, R., and Lin Y.L *Electrochim. Acta.* **2001** 46, 2843.

26. Kinoshita, K., Song, X., Kim, J., and Inaba, M. *J. of Power Sources* **1999** 81-82, 170.

3. Non-Limiting Hydrogen Electrosorption Properties of Asymmetric Palladium Nanoparticle-Modified Porous Carbon Electrodes

3.1 Introduction

Among the possible alternatives for fossil fuel based energy systems, hydrogen fuel remains attractive because of its great abundance and that it is considered a clean technology that causes minimal environmental pollution. The storage and transportation of hydrogen however still remains a great challenge. [1] The two main approaches for hydrogen storage are physical storage; such as compression or liquefaction of molecular hydrogen and adsorption into porous materials, and chemisorption which relies on materials that can form alloys and compounds with hydrogen. [2] Pressurized hydrogen tanks and cryogenic liquefied hydrogen are effective, resulting in storage volumes three times greater than gasoline, but the low volumetric density of hydrogen requires high pressures or low temperatures which makes these respective techniques cost prohibitive. [3] Chemisorption onto metals such as magnesium, lithium, and aluminum, and gases such as ammonia, can result in large gravimetric volumes of hydrogen stored but require energy-inefficient endothermic processes for release and are generally irreversible. [4] Solid state storage of hydrogen is often desirable because of high energy efficiencies, low heats of adsorption, fast adsorption/desorption kinetics, and good reversibility. [5] For this approach porous materials have become the materials of choice due to their enhanced adsorption properties towards gaseous molecules and the ability to tune the pore sizes for functionality. [6] Among this class of materials alumoscilicates and metal organic frameworks are widely studied as hydrogen storage materials because of their high porosity, low density, good crystallinity, and high surface area.

Nanostructured carbon materials can also be created with high specific areas that make them good candidates for hydrogen storage. [7] Activated carbons in particular have been reported as good gas adsorbents that include hierarchical carbon structures with nano/microporosity. Nanopores are used for enhanced ion adsorption while micropores can help promote quick transportation of hydrogen to the bulk of the material. [8] However, pure carbon still has a drawback in that high amounts of hydrogen adsorption are not favored at

room temperatures and cryogenic cooling is required. In order to overcome this, metal catalysts such as Pd are often used that cause catalytic breaking of hydrogen-hydrogen bonds. [9] The resulting hydrogen atoms can then diffuse into the palladium nanoparticle itself or, through a spillover mechanism, migrate to the carbon support and adsorb onto carbon active sites. [10]

Recently we have reported on novel hierarchical porous carbon structures fabricated out of pyrolyzed photoresist films by interferometric lithography. [11] The highly ordered carbon electrodes consist of five interconnected layers of interconnected hexagonal micropores with nanometer connecting spokes. These structures exhibit high mass transport profiles for certain redox analytes and hemispherical diffusion profiles over macroscopic volumetric areas. [12] We have also demonstrated that the unique properties of the pyrolyzed photoresist material can be used for the deposition of ultra small and highly dispersed Au, Pd, and Pt nanoparticles with narrow size distributions.[11-13] Because of the high hydrophobicity of the 3D porous structures the use of aqueous solutions result in nanoparticle depositions on only the top 2 – 2.5 layers while mixed acetonitrile/water solutions are necessary to achieve homogeneous nanoparticle depositions that coat all five interconnected layers. Herein we would like to report on the hydrogen electroadsorption properties of the homogeneous Pd-modified structures as well as unusual non-limiting adsorption onto the asymmetrically-modified Pd nano/microstructures.

3.2 Materials and Methods

Materials and Instruments. All solutions were prepared with 18 MΩ water using a Barnstead Nanopure water purifier (Boston, MA). Isopropanol, H_2SO_4, Acetonitrile, and $PdCl_2$ purchased from Sigma. All electrochemical measurements were performed on a CH Instruments 660 Electrochemical Analyzer (Austin, TX) and were measured versus an Ag/AgCl in 3M NaCl reference and a Pt counter electrode from Bioanalytical Systems (West Lafayette, IN). Scanning electron microscope (SEM) imaging was performed on a Zeiss Supra 55VP field emission gun scanning electron microscope.

Interferometric Lithography of 3D Porous Carbon Electrodes. A bottom anti-reflection coating (BARC), iCON-7 (Brewer Science, Rolla Missouri) was spun onto Silicon wafers at 3000 RPM and baked on a vacuum hotplate at 205°C for 60s. Negative tone NR7 from

Futurrex Inc. was used in all of the experiments. A thin layer of NR 7 100P (~ 100 nm) was deposited and spun at 3000 RPM to create an adhesion layer. After flood exposure and post exposure bake at 130 °C on a vacuum hotplate, a thick layer (6μm) of NR7-6000P was deposited and spun at 3000RPM and soft-baked at 130 °C. The frequency tripled 355 nm line of a Q-switched Nd:YAG laser was used to form the interference pattern. The beam was expanded and split into 2 separate beams and interfered with an angle of 32 degrees between the planewave propagation vectors. The plane of incidence contains both propagation vectors as well as the angle bisector of the propagation vectors, which is tilted with respect to the sample surface normal by 45 degrees. After each exposure the sample is rotated in the plane by 120 degrees and the process is repeated a total of 3 times. After exposure the sample received a post-exposure bake of 85 °C for 2 minutes on the vacuum hotplate. A 120 second puddle development, using RD-6 (Futurrex, Inc) and spin drying completed fabrication of the resist structures. The samples were baked on a hotplate at 180 °C for 30 minutes. The samples were then pyrolyzed at 1100 °C for 1 hour in forming gas (5% H_2 and 95% N_2). Substrates were rinsed with isopropoanol and water before use.

Palladium deposition. Pd was electrochemically deposited onto 3D porous carbon electrodes in both acidic water and mixture of acetonitrile/water solutions. The electrode potential was set right at the beginning of hydrogen evolution at carbon. The deposition was monitored by the increasing current due to Pd-induced hydrogen evolution.

3.2. Results and discussion

The homogeneous and asymmetric deposition of Pd nanoparticles was described previously. [12] Briefly, when depositions at -0.45 V from a 2 mM Pd/0.5 M H_2SO_4 aqueous solution (versus Ag/AgCl reference and Pt counter electrodes) are used the hydrophobicity of the carbon prevents the aqueous solution to access the bottom layers of the porous carbon and results in Pd deposition only on the top 2 – 2.5 layers, as shown in Figure 1A. Complete wetting, and thus full particle coverage, is accomplished in a MeCN:water mixture (90:10 vol%) (versus Ag/$AgNO_3$ reference and Pt counter electrodes), as shown in Figure 1B. These two electrodes differ greatly in their hydrogen electrosorption properties. Figure 2B shows characteristic hydrogen electrosorption on homogeneously-coated Pd electrodes scanned in 0.5M $HClO_4$. The electrode potential was held initially at a negative value where hydrogen

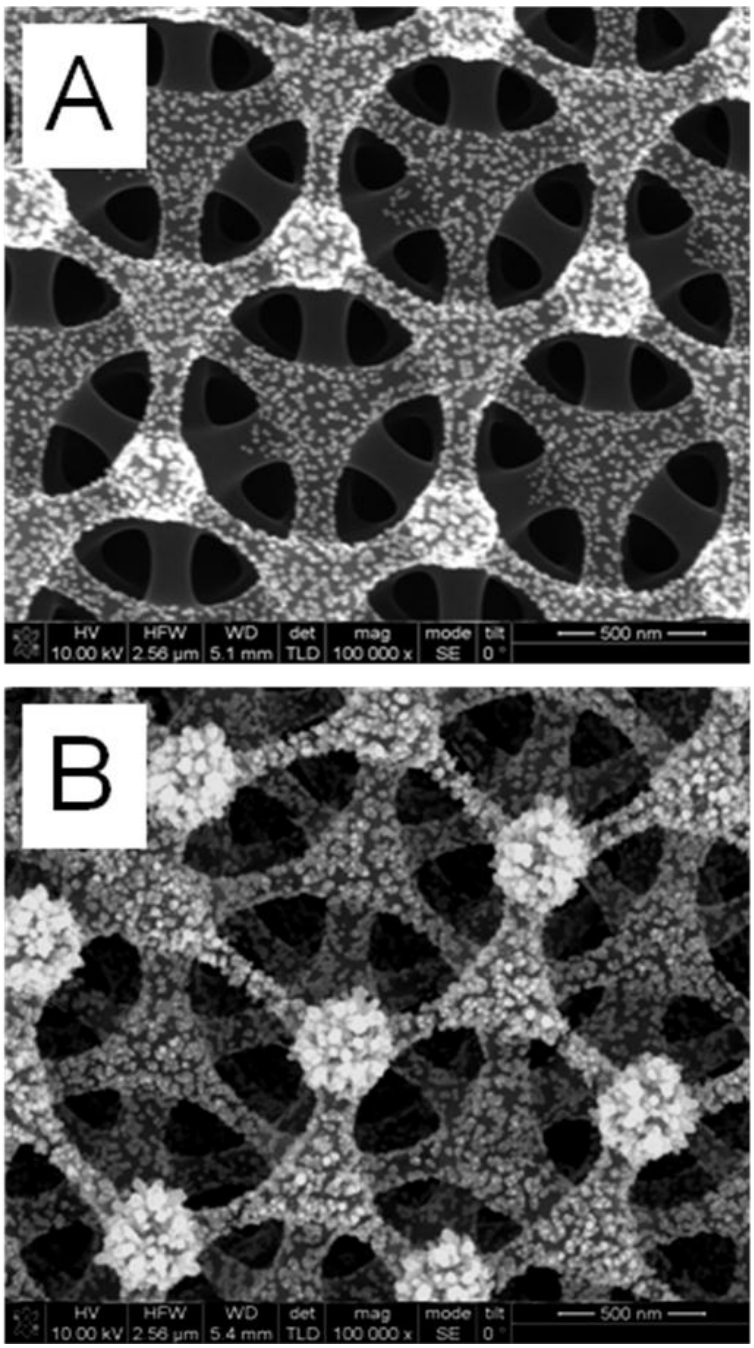

Figure 1. SEM images of Pd deposition at 3-D porous carbon electrodes. (A) deposition from 2mM Pd/0.5 M H2SO4, (B) deposition from 2 mM Pd/(MeCN + H_2O + 0.1 M HCl). Deposition potential: -0.45 V, deposition time: 100 s.

adsorption or absorption takes place, then was scanned anodically to produce a hydrogen desorption wave which provides quantitative data as to how much hydrogen was adsorbed/absorbed. A monolayer limited hydrogen adsorption profile was observed as long as the potential was held positive of -0.25 V. After -0.25 V a sharp transition was observed that indicates hydrogen absorption into the palladium crystallites which dominates the hydrogen desorption wave. Between -0.3 and -0.4 V the hydrogen absorption reaches a limiting value typically seen in many "limited volume electrodes" (LVEs), such as thin film electrodes. [14-16] Asymmetrically-coated Pd electrodes also exhibit monolayer hydrogen adsorption profiles like the homogeneous Pd electrodes up to -0.25 V (Figure 2A). Interestingly, the asymmetric electrodes do not show the same limiting values for hydrogen absorption. For instance, a large increase of the hydrogen desorption wave takes place between -0.35 V and -0.4 V (Figure 2A dashed line). Instead of behaving like a LVE for hydrogen absorption we believe that the hydrophobic carbon limits solution penetration in the asymmetric electrodes. In contrast, for the homogeneous coatings the hydrophobic carbon was completely covered by hydrophilic Pd particles, which were accessible to aqueous electrolyte. While the exact nature of this non-limiting volume effect is not yet elucidated we believe that it is reasonable to assume that the interstitial void in the bottom of the pores is responsible for this behavior. It is well known that hydrogen physisorption and chemisorption from the gas phase are fundamentally different than that in the liquid phase, and we believe that hydrogen spillover from the palladium nanoparticles could be undergoing a biphase adsorption/desorption process at the heterogenous gas/liquid junction causing the unusual non-limiting behavior.[17,18]

To further study hydrogen storage in the asymmetric electrodes and the influence of the hydrophobic pores, we investigated hydrogen adsorption and absorption on electrodes which were created using short deposition times, shown in Figure 3. At a deposition time of 10 s (in 90 %acetonitrile/10 % water) the Pd particles still deposited throughout the entire porous structures but were dramatically less dense (Figure 3 left inset) than the 100 sec deposition times for the homogeneous electrodes described above. In this case the hydrogen adsorption is limiting within a monolayer until -0.25 V, yet the hydrogen absorption wave does not reach a saturation value upon negatively shifting the potential. We also observed that the

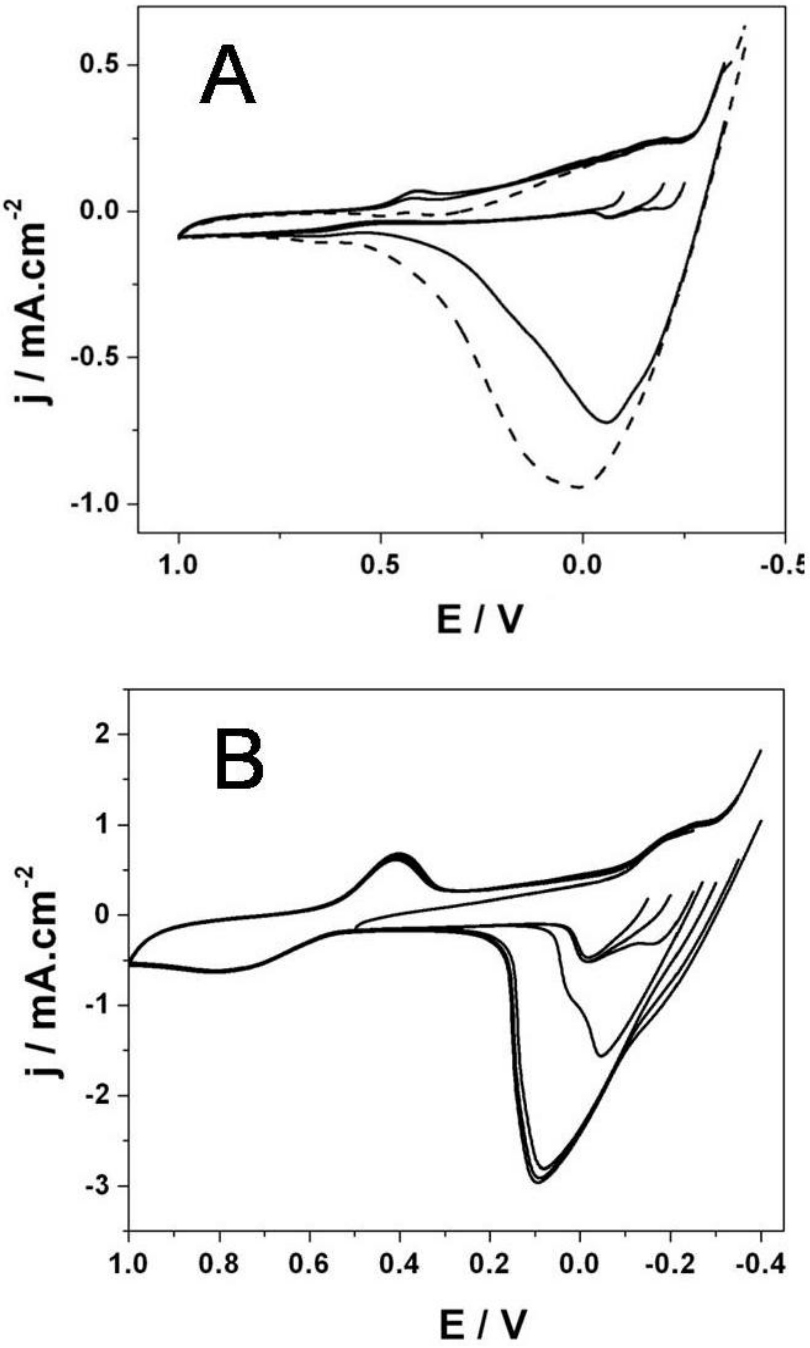

Figure 2. Cyclic voltammograms of Pd nanoparticle modified 3D carbon electrodes, (A) Homeogeneous and (B) Assymetric in 0.5 M $HClO_4$. The electrodes were initially held at individual electrode potentials for 60 s then scanned positively. Scan rate: 50 mV/s.

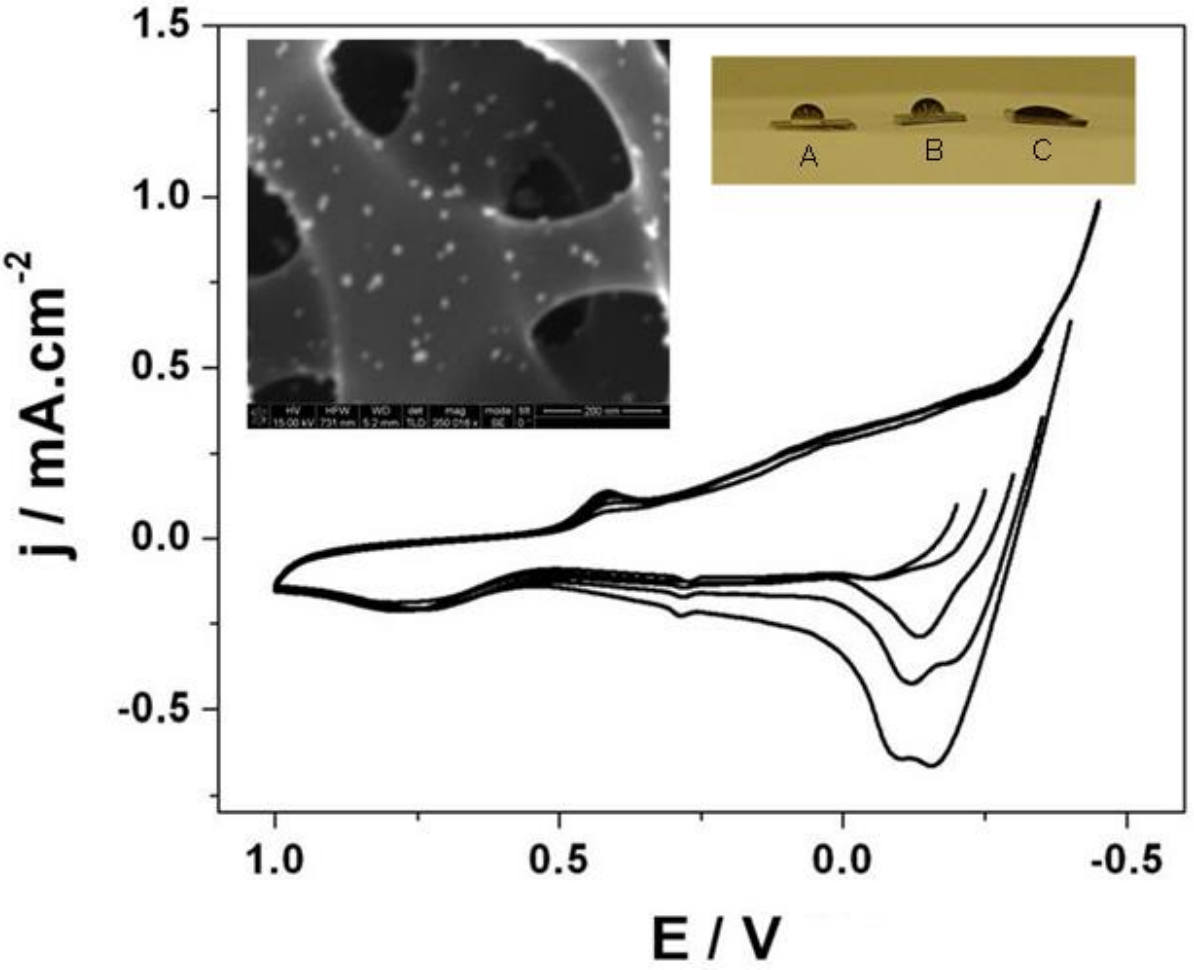

Figure 3. Cyclic voltammograms of Pd nanoparticle modified 3D carbon electrode in 0.5 M $HClO_4$. The electrode was initially held at individual electrode potentials for 60 s then scanned positively. Pd deposition time: 10 s. Scan rate: 50 mV/s. Insert (left) picture is the corresponding SEM image of the electrode. Insert (right) Contact angles from 20 μl drops of deionized water placed onto bare 3D carbon electrode , and 3D carbon electrode after 10, and 100 sec of Pd deposition from 2 mM Pd/(Actenonitrile + H_2O + 0.1 M HCl) A, B, and C respectively. Deposition potential: -0.45 V

hydrogen absorption profile increases with increased polarization times up to 200 s at polarization potentials more negative than -0.25V. We reasonably assume that due to the low density of Pd particles the hydrophobic nature of the carbon dominates, despite the homogeneous deposition of the particles throughout the pores, leading to incomplete solution penetration resulting in similar hydrogen absorption characteristics as the asymmetric Pd electrodes. The hydrophobicity of this surface is supported by contact angle measurements that show a similar profile for repulsion of water droplets between the bare porous carbon and the same surface after 10 sec of Pd deposition. In contrast, after 100 sec of Pd deposition the surface becomes notably more hydrophilic (Figure 3 right inset). In control experiments, no hydrogen desorption peaks were observed on the bare 3D porous carbon electrodes indicating that the Pd particles are necessary to catalyze hydrogen formation (Figure 4).

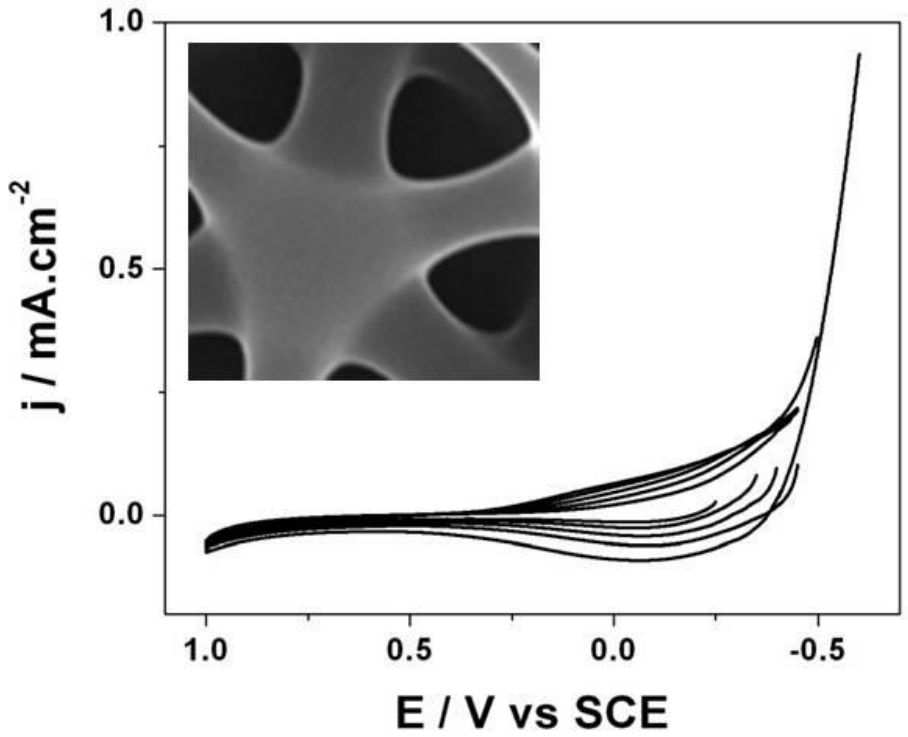

Figure 4. Cyclic voltammograms of bare 3D carbon electrode in 0.5 M $HClO_4$. The electrode was initially held at individual electrode potentials for 60 s then scanned positively. Scan rate: 50 mV/s. The insert picture is the corresponding SEM image of the electrode.

3.3 Conclusions

In summary, we present results showing the hydrogen electrosorption properties in high density homogeneous, asymmetric, and low density homogeneous Pd-modified 3D porous carbon electrodes. Homogeneously modified high density Pd electrodes showed typical hydrogen adsorption profiles as expected for limited volume electrodes and could be promising candidates for micro-energy devices such as hydrogen based fuel cells. In contrast, asymmetrically-modified electrodes and low density homogeneous Pd-modified electrodes exhibited unusual non-limiting adsorption profiles which we believe to be due to the heterogeneous gas/liquid interface that is a result of the hydrophobic properties of the underlying carbon electrode and the unique 3D porous structure.

3.4 References

[1] J. Graetz, Chem. Soc. Rev. 38 (2009) 73-82

[2] U. Eberle, M. Felderhoff, F. Schuth, Angew. Chem. Int. Ed. 48 (2009) 6608-6630

[3] V. Meregalli, M. Parrinello, Appl. Physics A 72 (2001) 143-146

[4] S. Harder, J. Spielman, J. Intemann, H. Bandmann, Angew. Chem. In. Ed. 50 (2011) 4156-4160

[5] C. Weidenthaler, M. Felderhoff, Energy Environm. Sci. 4 (2011) 2495-2502

[6] J. Germain, J.M.J. Frechet, F. Svec, Small 5 (2009) 1098-1111

[7] B. Assfour, S. Leoni, G. Seifert, I.A. Baburin, Adv. Mat. 23 (2011) 1237-1241

[8] B. Fang, M. Kim, J.H. Kim, J.S. Yu, Langmuir 24 (2008) 12068-12072

[9] A. Halder, S, Patra, B. Viswanath, N. Munichandraiah, N. Ravishankar, Nanoscale 3 (2011) 725-730

[10] B.D. Adamas, C. K. Ostrom, S. Chen, A. Chen, J. Phys. Chem. C 114 (2010) 19875-19882

[11] D.B. Burckel, C.M. Washburn, A.K. Raub, S.R.J. Brueck, D.R. Wheeler, S.M. Brozik, R. Polsky, Small 5 (2009) 2792

[12] X. Xiao, M.E. Roberts, D.R. Wheeler, C.M. Washburn, T.L. Edwards, S.M. Brozik, G.A. Montano, B.C. Bunker, D.B. Burckel, R. Polsky, ACS Appl. Mat. And Int. 2 (2010) 3179

[13] S. Sattayasamitsathit, A.M. O'Mahony, X. Xiao, S.M. Brozik, C.M. Washburn, D.R. Wheeler, J.C. Cha, D.B. Burckel, R. Polsky, J. Wang, Electrochem. Comm. 13 (2011) 856-860

[14] A. Czerwinski, I. Kiersztyn, M. Grden, J. Czapla, J. Electroanal. Chem 471 (1999) 190-195.

[15] B. Adams, C. Ostrom, A. Chen, Langmuir 26 (2010) 7632-7637

[16] P. Piela, Z. Rogulski, M. Krebs, E. Pytlik, M. Scmalz, J. Dlubak, M. Karwowska, A. Gumkowska, A. Czerwinski, J. Electroanal. Soc. 157 (2010) A254-A258

[17] A. Dillon, M.J. Heben, Appl. Phys. A 72 (2001) 133-142

[18] G. Jerkiewicz, A. Zolfaghari, J. Electrochem. Soc. 4 (1996) 1240

DISTRIBUTION LIST

1	MS 0899	RIM-Reports Management, 9532
1	MS 0359	Donna Chavez, LDRD office, 1911